International Journal of Heat and Mass Transfer 52 (2009) 151–164

Contents lists available at ScienceDirect

International Journal of Heat and Mass Transfer

journal homepage: www.elsevier.com/locate/ijhmt

Effects of variable density for film evaporation on laminar mixed convection in a vertical channel

N. Laaroussi [a], G. Lauriat [a,*], G. Desrayaud [b]

[a] Université Paris-Est, Laboratoire Modélisation et Simulation Multi Echelle, MSME FRE 3160 CNRS, 5 bd Descartes, F-77454 Marne-la-Vallée Cedex, France
[b] Université de Picardie, Laboratoire Modélisation et Simulation Multi Echelle, MSME FRE 3160 CNRS, 48 rue Raspail, BP 422, F-02109 Saint-Quentin Cedex, France

ARTICLE INFO

Article history:
Received 29 January 2008
Received in revised form 7 May 2008
Available online 23 July 2008

Keywords:
Vertical channel
Surface condensation
Mixed convection
Numerical heat transfer

ABSTRACT

A numerical investigation was conducted to study mixed convection in a vertical parallel-plate channel with evaporation of thin liquid films on wetted walls. Air–water vapor and air–hexane vapor mixtures, assumed as ideal gases, are considered under various boundary conditions. Steady laminar, two-dimensional flows are examined in detail for large mixture density changes between the inlet and outlet sections of the channel. Comparisons with the usual problem formulations based on the Boussinesq approximation are discussed. The elliptic flow model used allow to predict flow reversal as well as recirculation cells in the entrance region. The evaporation of water and hexane into a downward laminar stream of dry air leads to various flow structures according to the interfacial mass fraction, $W_{v,w}$, and differences in the molecular weights of the species. For water evaporation, the thermal and solutal forces are opposing. In the entrance region, evaporation produces a significant increase in axial velocity at the core region in comparison with pure forced flow. For $W_{v,w}$ larger than $\approx$0.2, upward velocities may be observed in the wall regions due to solutal buoyancy forces near the wetted surfaces. For hexane evaporation, the solutal force acts downward. Mass diffusion produces both a strong flow acceleration in the boundary layers and flow recirculations at the channel center for large mass evaporation rates.

1. Introduction

Natural and mixed convection combined with film evaporation or condensation in vertical open channel flows have received considerable attention because they are important in many processes occurring in nature and engineering applications. For example, the so-called evaporating cooling is encountered in engineering applications such as humidity control systems, cooling of electronic equipment, design of cooling towers, protection of system components from a high temperature gas stream, and many others. When the channel wall is wetted by a thin liquid film, large heat transfer augmentation can be expected because of the simultaneous presence of thermal and mass diffusion buoyancy forces resulting from density variations due to temperature and concentration gradients in conjunction with film vaporization.

Pioneer studies by Somers [1] and Nakamura [2] dealt with the problem of simultaneous transfers of sensible and latent heat in the case of evaporative cooling in a natural convection boundary layer over a flat plate. Somers employed an approximate integral method and Nakaruma neglected buoyancy forces caused by binary diffusion. Both of these authors assumed constant physical properties and neglected the effects of differences in specie enthalpy. This work was reconsidered by Chow and Chung [3] for evaporation of water into a laminar stream of air, superheated steam and a mixture of the two. They examined, in particular, the physical reasons for the existence of the inversion temperature by using a similarity approach and the relevance of the one-third rule approximation [4]. In an experimental study, Haji and Chow [5] confirmed in part these analytical results. Lee et al. [6] examined experimentally and numerically natural convection in a channel formed between two vertical plates, one porous and the other impermeable. Both plates were maintained at uniform temperatures, higher than the ambient, and a heavy gas (CO_2) was transpired into the channel through the porous plate. The negative buoyancy of the gas resulted in a downward flow along the porous plate, while heat transfer at the impermeable plate caused an upward flow. Chang et al. [7] investigated the effects of the coupled thermal and mass diffusion on the steady development of natural convection flows of air–water vapor mixtures in a finite, vertical tube. The effects of tube length and differences between entry and wall temperatures were examined in detail. Particular attention was paid to studying the heat transfer enhancement when the buoyancy forces are in the same direction ($T_w > T_0$) and the reduction of heat transfer when the flow is retarded ($T_w < T_0$). However, the use of the Boussinesq approximation renders these results applicable only for low concentrations of water vapor.

* Corresponding author. Tel.: +33 1 6095 7269; fax: +33 1 6095 7294.
E-mail address: lauriat@univ-mlv.fr (G. Lauriat).

0017-9310/$ - see front matter © 2008 Elsevier Ltd. All rights reserved.
doi:10.1016/j.ijheatmasstransfer.2008.05.022

Nomenclature

a	thermal diffusivity [$m^2\ s^{-1}$]
A	aspect ratio, $= L/2d$
C_p	specific heat [$J\ K^{-1}\ kg^{-1}$]
$D_h = 4d$	hydraulic diameter [m]
d	half distance between walls [m]
$D_{v,m}$	binary mass diffusion coefficient [$m^2\ s^{-1}$]
g	gravitational acceleration [$m\ s^{-2}$]
Gr_M	solutal Grashof number, $Gr_M = g\beta_M(W_w - W_0)D_h^3/\nu_m^2$
Gr_T	thermal Grashof number, $Gr_T = g\beta_T(T_w - T_0)D_h^3/\nu_m^2$
h	enthalpy [$J\ kg^{-1}$]
$\bar{h}$	mixture enthalpy [$J\ kg^{-1}$]
h_{lv}	latent heat [$J\ kg^{-1}$]
L	channel length [m]
k	thermal conductivity [$W\ m^{-1}\ K^{-1}$]
$\dot{m}$	mass flow rate [$kg\ s^{-1}$]
$\phi_{m,v}$	mass flow rate of vapor condensed or evaporated per unit length [$kg\ s^{-1}$]
M	molecular weight [kg/kmol]
N	Buoyancy parameter $N = Gr_M/Gr_T = Ri_M/Ri_T$
$\overline{Nu}$	average Nusselt number based on cavity width
p	dynamic pressure [Pa]
p_{vs}	saturation pressure of vapor [Pa]
P	thermodynamic pressure [Pa]
Pr	mixture Prandtl number, $= \nu_m/a_m$
q_w	cold wall heat flux density [$W\ m^{-2}$]
R	universal gas constant, $= 8.315$ kJ $kmol^{-1}$
Re	Reynolds number $Re = U_0 D_h/\nu$
Ri_M	solutal Richardson number $Ri_M = Gr_M/Re^2$
Ri_T	thermal Richardson number $Ri_T = Gr_T/Re^2$
Sc	Schmidt number $Sc = \nu/D_{v,m}$
T	temperature [K]
$\vec{V} = (u, v)$	velocity vector [$m\ s^{-1}$]
W	mass fraction
(x, y)	coordinates [m]

Greek symbols

β_M	solutal coefficient of volumetric expansion
β_T	thermal coefficient of volumetric expansion [K^{-1}] $\beta_T = 1/T_r$
ΔT	temperature difference, $= (T_0 - T_w)$ [K]
ϕ_0	relative humidity of moist air [%]
μ_m	mixture dynamic viscosity [$N\ m^{-1}\ s^{-1}$]
Ψ	streamfunction
ρ	density [$kg\ m^{-3}$]
$\bar{\bar{\tau}}$	viscous stress tensor
ξ	stretching parameter

Subscripts

a	dry air
w	wall
m	mixture
M	solutal
T	thermal
v	vapor
∞	ambient fluid

Superscript

–	average quantity

Yan and Lin [8] presented a pioneer study on the effects of liquid film evaporation from a wetted wall of a vertical parallel-plate channel. Great attention was given to the role of latent heat transfer in laminar mixed convection. Lin et al. [9] studied the role of vaporization of a thin film of liquid water on a vertical tube wall in laminar mixed convection. They showed that heat transfer in the flow is dominated by the transport of latent heat and that there exists a wall temperature T_w at which the ratio of the latent heat flux to the sensible heat flux is at a minimum. The heat transfer enhancement through latent heat transport in mixed convection flows between vertical plates was reconsidered by Yan [10] for air–water and air–ethanol mixtures with variations of the thermophysical properties taken into account. The results showed that there was a larger heat transfer enhancement for a channel wetted by an ethanol film than for one wetted by a water film. Vaporization or condensation of water vapor on the wetted channel walls in laminar mixed convection in a vertical plate channel with asymmetric heating was investigated by Yan et al. [11]. The results showed anew that heat transfer is dominated by the transport of latent heat.

Tsay and Lin [12] performed a numerical analysis to explore heat and mass transfer in a laminar gas stream flowing over a falling liquid film. The conservation equations for the liquid film and gas stream coupled through interfacial matching conditions were simultaneously solved. It was shown in particular that the predicted results obtained by including transport in the liquid film were contrasted with those where the liquid film transport was untreated. It was concluded that the assumption of an extremely thin film is only valid for a system with a small liquid mass flow rate. Yan and Lin [13] and Yan [14] extended the analysis of the effects of the finite liquid films in the case of turbulent natural convection with evaporation in vertical plate channels and tubes. The influences of the liquid flow rate were investigated in great detail. Their results indicated that the influence of a laminar falling film is small in the core region, while it is rather substantial near the gas–liquid interface. Yan and co-workers [15–17] presented numerical studies for both laminar and turbulent mixed convection in vertical plate channels. The major conclusions drawn in these papers are increases in heat transfer as the mass flow rate of the liquid film decreases.

Recently, mixed convection in the entrance region of a vertical or an inclined rectangular duct with film evaporation along a porous wall was considered [18,19]. The Boussinesq approximation was invoked and the thermophysical properties of humid air were assumed to be constant (except for the density variation in the buoyancy term) and evaluated by the one-third rule as in [9]. A vorticity–velocity formulation of the three-dimensional Navier–Stokes equations was introduced and the axial diffusion terms were neglected in the momentum, energy and mass conservation equations. The effects of the wetted wall temperature, Reynolds number, relative humidity of the moist air and aspect ratio were examined in detail. The major results obtained, except those for the aspect ratio, confirmed the conclusions drawn previously when the thin liquid film approximation is retained.

In all the above mentioned work, the problem was studied for various thermal boundary conditions but by systematically using boundary-layer type formulations or by neglecting axial diffusion of the various flow quantities. However, full elliptical formulations are required for the prediction of possible flow reversal. The first work dealing with heat and mass transfer for binary fluids flowing in a vertical plate channel in which a two-

dimensional elliptical formulation was used seems to have been conducted by Desrayaud and Lauriat [20]. A steady, laminar Boussinesq natural convective flow of an ideal air–water vapor mixture was considered in the cases of small temperature variations and low concentrations of vapor. New correlations were derived for the latent and sensible Nusselt numbers and the similarity between the Sherwood number and Nusselt number was emphasized in the framework of the assumptions introduced in the mathematical formulation (condensation of a vapor with an incondensable carrier gas, low ranges of mass vapor concentration in the core flow region). Laminar mixed convection of the downward flow of humid air in a vertical channel with isothermal wetted walls at a temperature lower than the entering air was studied numerically by Hammou et al. [21]. The inlet conditions were such that condensation or evaporation at the walls may occur. However, the inlet and wall thermal boundary conditions were for relatively small effects of phase change on the flow field owing to the low mass fraction of water vapor in the flow core. The problem was reconsidered recently in [22] for both upward and downward mixed convection. The results show that natural convection can increase or decrease the sensible and latent heat fluxes according to the flow direction. Flow reversal was shown for upward flows in the case of relatively high temperature differences between ambient and isothermal walls. However, no clear results were shown about the existence of flow reversal for flows of humid air at low water vapor concentration.

The above literature survey shows that the elliptic formulation has been systematically applied for constant density flows, i.e., for mixtures with small concentrations of species carried by an incondensable gas. In these cases, the Boussinesq approximation may be quite accurately applied. On the other hand, for flows of a gas over vaporizing wall liquid films with large differences in molecular weight, the section averaged mixture density may increase or decrease in the upstream direction according to the ratio of the components' molecular weights. In that case, the assumption of constant density flow is highly questionable when the vaporized species cannot be treated as a dilute component. Therefore, a key point in the problem of interest is whether it is possible or not to use a constant density formulation. In the present paper, we address this question by considering laminar mixed convection with film evaporation of water and hexane. We performed a numerical analysis by solving the conservation equations for a binary mixture of ideal gas with all the thermophysical properties varying with temperature and concentration. The physical system investigated is a vertical parallel-plate channel wetted by a thin liquid film at constant temperature as shown schematically in Fig. 1. The film is exposed to a laminar air stream with constant inlet velocity, temperature and vapor concentration. Since the buoyancy effects due to thermal and solutal forces are accounted for, mixed convective flows with various Richardson numbers based on reference quantities are studied. It is shown that a constant density formulation may lead to highly inaccurate results when the reference temperature and concentration are not properly chosen and that a flow reversal may occur in the entrance channel region provided that the vaporizing component is much heavier than the carrier gas.

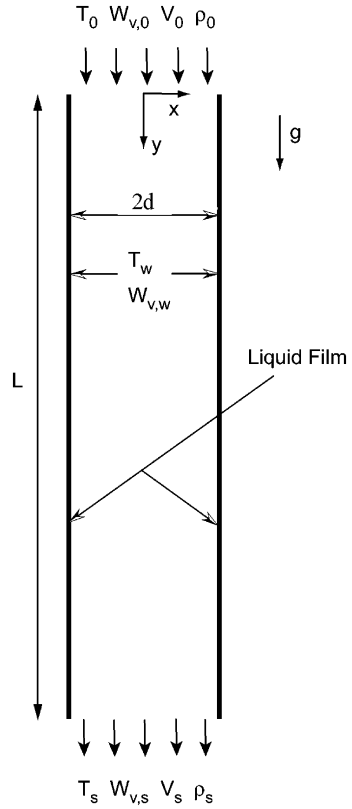

Fig. 1. Schematic diagram of the channel and coordinate system.

2. Problem statement

We consider steady, developing, downward laminar flow of a vapor–air mixture within a vertical plate channel with the wall maintained at constant temperature, T_w. At the inlet section, the axial velocity V_0, temperature T_0, vapor mass fraction $W_{v,0}$ and mixture density $\rho_{m,0}$ are uniform. The fluid can be either a mixture in the overheated state $(W_{v,0} < 1)$ or dry air as a limiting test case $(W_{v,0} = 0)$. It is assumed that the liquid films are extremely thin so that boundary conditions for heat and mass transfer can be introduced as was suggested by Lin et al. [9]. Furthermore, the solubility of air in liquid films is considered as negligibly small and the normal direction velocity of air is zero at the interfaces, the interface is at thermodynamic equilibrium and the total heat transfer from the interface into the gas stream results from sensible, latent and interdiffusion fluxes. Dufour and Soret effects are neglected and there are no chemical reactions, heat dissipation or fog formation inside the channel. In view of the large number of variables and parameters involved in the problem formulation, the governing equations were not cast in dimensionless form. However, relevant dimensionless numbers such as Lewis number, Reynolds, thermal and solutal Rayleigh numbers based on reference quantities were monitored in order to coarsely determine the relative effects of various terms.

The continuity equation reads:

$$\frac{\partial(\rho_m u)}{\partial x} + \frac{\partial(\rho_m v)}{\partial y} = 0 \tag{1}$$

The momentum equation is written as

- x-direction

$$\rho_m u\frac{\partial u}{\partial x} + \rho_m v\frac{\partial u}{\partial y} = -\frac{\partial p}{\partial x} + \frac{\partial}{\partial x}\left(\mu_m\frac{\partial u}{\partial x}\right) + \frac{\partial}{\partial y}\left(\mu_m\frac{\partial u}{\partial y}\right) + \frac{\partial}{\partial x}\left[\mu_m\frac{\partial u}{\partial x} - \frac{2}{3}\mu_m\left(\frac{\partial u}{\partial x} + \frac{\partial v}{\partial y}\right)\right] + \frac{\partial}{\partial y}\left(\mu_m\frac{\partial v}{\partial x}\right) \tag{2}$$

- y-direction

$$\rho_m u\frac{\partial v}{\partial x}+\rho_m v\frac{\partial v}{\partial y}=-\frac{\partial p}{\partial y}+\frac{\partial}{\partial x}\left(\mu_m\frac{\partial v}{\partial x}\right)+\frac{\partial}{\partial y}\left(\mu_m\frac{\partial v}{\partial y}\right)+\frac{\partial}{\partial y}\left[\mu_m\frac{\partial v}{\partial y}-\frac{2}{3}\mu_m\left(\frac{\partial u}{\partial x}+\frac{\partial v}{\partial y}\right)\right]+\frac{\partial}{\partial x}\left(\mu_m\frac{\partial u}{\partial y}\right)+\rho_m(T,W_v)g \quad (3)$$

For a binary mixture, the energy equation written in terms of enthalpy only is

$$\frac{\partial(\rho_m u\bar{h})}{\partial x}+\frac{\partial(\rho_m v\bar{h})}{\partial y}=\frac{\partial}{\partial x}\left(\frac{k_m}{\overline{C_p}}\frac{\partial\bar{h}}{\partial x}\right)+\frac{\partial}{\partial y}\left(\frac{k_m}{\overline{C_p}}\frac{\partial\bar{h}}{\partial y}\right)+\frac{\partial}{\partial x}\left(\rho_m(h_v-h_a)D_{v,m}\frac{\partial W_v}{\partial x}\right)+\frac{\partial}{\partial y}\left(\rho_m(h_v-h_a)D_{v,m}\frac{\partial W_v}{\partial y}\right) \quad (4)$$

where $\bar{h}$ is the total enthalpy of the mixture, $\rho_m\bar{h}=\rho_v h_v+\rho_a h_a$, and $d\bar{h}=\overline{C}_p\,dT$. The second term of the right-hand side of the energy equation represents the contribution on the energy flux due to interdiffusion of species mixture with air and liquid vapor having different enthalpies. The enthalpy of specie "i" is

$$h_i=h_i^0+\int_{T_0}^{T}C_{p,i}\,dT \quad (5)$$

If the enthalpy of "i" at $T_0=0$ K is arbitrarily taken as zero

$$\bar{h}=(1-W_v)\int_0^T C_{p,a}\,dT+W_v\int_0^T C_{p,v}\,dT \quad (6)$$

For an ideal gas mixture, $d\bar{h}=\overline{C_p}\,dT$ (where $\overline{C_p}$ is a function of temperature only). Therefore, $(k_m/\overline{C_p})\nabla\bar{h}=k_m\nabla T$. The energy equation can thus be written as

$$\frac{\partial(\rho_m u\bar{h})}{\partial x}+\frac{\partial(\rho_m v\bar{h})}{\partial y}=\frac{\partial}{\partial x}\left(k_m\frac{\partial T}{\partial x}\right)+\frac{\partial}{\partial y}\left(k_m\frac{\partial T}{\partial y}\right)+\frac{\partial}{\partial x}\left(\rho_m(h_v-h_a)D_{v,m}\frac{\partial W_v}{\partial x}\right)+\frac{\partial}{\partial y}\left(\rho_m(h_v-h_a)D_{v,m}\frac{\partial W_v}{\partial y}\right) \quad (7)$$

The mass species equation for the vapor is

$$\frac{\partial(\rho_m uW_v)}{\partial x}+\frac{\partial(\rho_m vW_v)}{\partial y}=\frac{\partial}{\partial x}\left(\rho_m D_{v,m}\frac{\partial W_v}{\partial x}\right)+\frac{\partial}{\partial y}\left(\rho_m D_{v,m}\frac{\partial W_v}{\partial y}\right) \quad (8)$$

It should be mentioned that in the above equations all the thermophysical properties depend on the mixture temperature and concentration of each component. Since we are considering a perfect gas mixture, the dynamic viscosity, thermal conductivity and coefficient of thermal expansion of each component do not depend on pressure according to the kinetic theory.

The system of conservation equations is completed by the ideal gas law used for the calculations of the mixture density field:

$$\rho_m=\frac{PM_t}{RT} \quad (9)$$

where P is the thermodynamic pressure. For gas flows within a vertical channel having a height of the order of 1 m, it can be assumed that $P\approx P_a$, P_a being the ambient pressure. The molecular weight of the mixture is given by

$$\frac{1}{M_t}=\left(\frac{W_v}{M_v}+\frac{1-W_v}{M_a}\right) \quad (10)$$

Boundary conditions:

By assuming that the gas mixture-liquid film interface is in thermodynamic equilibrium, the interfacial mass fraction of vapor is related to the pressure of the vapor at saturation condition through the equation

$$W_{v,w}=\frac{p_{vs}(T_w)}{P}\frac{M_v}{M_t} \quad (11)$$

where $p_{vs}(T_w)$ is the saturation vapor pressure at the wall temperature.

Liquid evaporation produces a normal velocity of vapor which is calculated from the expression of the interfacial mass flux given by the Fick law. The following expression of the normal velocity component at liquid-mixture interface along wall assumes that the solubility of air in liquid is negligibly small and that the liquid film is stationary:

$$\vec{V}.\vec{t}_i=0,\quad \vec{V}.\vec{n}_i=-\frac{D_{v,m}}{(1-W_{v,i})}\frac{\partial W_v}{\partial n_i} \quad (12)$$

where $\vec{t}_i$ denotes the tangent vector along the interface and $\partial/\partial n_i$ the gradient in the direction of the outward normal $\vec{n}_i$ to the interface. Since the liquid film at the wall surface is assumed to be of negligible thickness, it is considered that the wall temperature can be used as the thermal boundary condition. Thus

$$T(x,y)=T_w \quad \text{at} \quad x=\pm d \quad \forall y \quad (13)$$

At the channel inlet ($y=0$ and $-d\leqslant x\leqslant d$), the pressure is related to the inlet velocity via the Bernoulli equation:

$$u=0,\ v=V_0,\ p=P_a+\frac{1}{2}\rho_{m,0}V_0^2,\ T=T_0 \quad \text{and} \quad W_v=W_{v,0} \quad (14)$$

At the channel exit ($y=L$ and $-d\leqslant x\leqslant d$), the flow is assumed to behave as a free jet which expands in a local hydrostatic pressure field at the exit elevation. The other flow conditions applied at the channel exit assume a zero axial gradient for velocity components, temperature and vapor mass fraction. However, if flow reversal occurs at the outlet ($v<0$), the boundary conditions for temperature and mass fraction are taken as the ambient conditions on the part of the section where $v<0$.

The use of elliptic equations (needed to account for the occurrence of recirculation) requires boundary conditions to be set, and at the outlet, zero normal gradients are usually assumed as boundary conditions. However, these locally parabolic outlet boundary conditions are not always well suited for developing flows or outlet recirculation (in this case, the boundary conditions are modified, but only on the re-entering ambient fluid boundary), but they are nevertheless used [20–22]. Another solution is to neglect axial diffusion of heat and momentum, the flow being assumed parabolic, giving the opportunity to use a marching procedure and eliminating the need for boundary conditions at the outlet [6–8,13,15–19]. But in this case, flow reversals cannot be predicted and therefore cannot be used in the present study.

2.1. Average quantities

The following averages of flow quantities were calculated for improving the analysis of the numerical solutions and will be discussed in Section 4. The averages output over the channel cross-section are the average velocity and relative humidity defined as

$$\overline{V}_m(y)=\frac{1}{2d}\int_{-d}^{d}v(x,y)\,dx,\quad \bar{\phi}(y)=\frac{1}{2d}\int_{-d}^{d}\phi(x,y)\,dx \quad (15)$$

The weighted-average quantities of interest are the bulk mixture density, temperature and liquid–vapor mass fraction

$$\bar{\rho}_m = \frac{\int_{-d}^{d} \rho_m v\,dx}{\int_{-d}^{d} v\,dx}, \quad \overline{T}_m = \frac{\int_{-d}^{d} \rho_m T v\,dx}{\int_{-d}^{d} \rho_m v\,dx}, \quad \overline{W}_v = \frac{\int_{-d}^{d} \rho_m W_v v\,dx}{\int_{-d}^{d} \rho_m v\,dx} \tag{16}$$

The local flux at the wall depends on three factors: the temperature gradient at the wall, the rate of mass transfer and species interdiffusion. These three contributions result in sensible heat transfer, latent heat transfer and species interdiffusion flux, respectively. Therefore, the total heat flux from the wet wall can be expressed as

$$q_w = -k_m \frac{\partial T_m}{\partial x} + \frac{\rho_m D_{v,m} h_{lv}}{(1-W_v)} \frac{\partial W_v}{\partial x} - (h_v - h_a)\rho_m D_{v,m} \frac{\partial W_v}{\partial x} \tag{17}$$

The sensible and latent local Nusselt numbers over the wetted wall can be written as

$$Nu_s(y) = -\frac{4d}{T_w - T_m(y)} \left.\frac{\partial T}{\partial x}\right|_w \tag{18}$$

$$Nu_l(y) = \frac{4d}{T_w - T_m(y)} \frac{\rho_m D_{v,m} h_{lv}}{k_r(1-W_{v,w})} \left.\frac{\partial W_v}{\partial x}\right|_w \tag{19}$$

The mass flux balance between $y = 0$ et y reads

$$\Phi_{m,v}(y) = 2\int_0^y \rho_m u_w\,dy = -2\int_0^y \rho_m \frac{D_{v,m}}{(1-W_{v,w})} \left.\frac{\partial W_v}{\partial x}\right|_{-d} dy \tag{20}$$

One of the constraints to be satisfied is the overall mass balance for mixture at every longitudinal location, that is

$$\Delta\dot{m}(y) = \int_{-d}^{d} (\rho_m(x,0)v(x,0) - \rho_m(x,y)v(x,y))\,dx = \Phi_{m,v}(y) \tag{21}$$

2.2. Boussinesq equations

The Boussinesq approximation was invoked in [11,22] although the model has restrictions of small temperature differences $\Delta T_{max}/T_r < 0.1$ and low mass fraction of vapor in the flow core. Therefore, the density variation was assumed to be important only in the buoyancy force term and modeled as a linear function of temperature and mass fraction. In addition, the thermophysical properties of the mixture were evaluated at reference temperature and mass fraction given by the 1/3 law from the expression given by Fujii et al. [23] (see also Lin et al. [9]). For double diffusion problems the thermal Grashof number Gr_T and the solutal Grashof number Gr_M may be introduced. The buoyancy parameter, N, is defined as:

$$N = \frac{Gr_M}{Gr_T} = \frac{\beta_M(W_{v,w} - W_{v,0})}{\beta_T(T_w - T_0)} \tag{22}$$

where

$$\beta_T = 1/T_0, \quad \beta_M = \frac{M_a}{M_v} - 1 \tag{23}$$

The solutal and thermal buoyancy forces act in the same direction when $N > 0$ and in opposing directions when $N < 0$.

3. Solution procedure

Calculations were carried out by utilizing the commercial, control-volume based code FLUENT 6.3 (Fluent Inc.). Results of the simulations were collected and processed by employing in-house softwares. A second-order upwind scheme was used for the advective and transport terms. The velocity–pressure coupling was solved with the PISO algorithm and the pressure was calculated with a body-force weighted scheme (Fluent 6.3 User's Guide). The governing equations were solved sequentially with a decoupled implicit scheme. Since imposition of the above mass flux boundary conditions is not available, user-defined functions (UDFs) called at each iteration were written. With this approach, no-slip boundary conditions were applied at the walls and source terms were introduced in the cells adjacent to the walls for the mass (mixture and species) conservation equations to account for vaporization of the liquid film. The source term added in the mass conservation equations was

$$S_m = \dot{m}_v \times \frac{A_G}{V_G} = -\frac{\rho_m D_{v,m}}{(1-W_v)} \frac{\partial W_v}{\partial x} \times \frac{A_G}{V_G} \tag{24}$$

where A_G and V_G are the surface and volume of the cell where the source term is introduced. Similarly, a source term $S_v = S_m$ was added in the mass conservation equation for vapor. These terms stand for the velocity boundary condition given in Eq. (12).

The calculation domain was mapped with rectangular structured grids refined in both directions to ensure high densities near the channel walls and in the inlet region where high gradients exist. Grid independence tests were performed using different grid sizes for various Reynolds numbers, ranging from $Re = 300$ to $Re = 900$, and interfacial mass fractions of water vapor or hexane vapor in the case of a channel aspect ratio $L/2d = 100$. The tests showed that local flow variables, such as downward velocities, mass fractions or temperatures at typical locations, and overall quantities such as the mass of liquid vaporized at the walls were relatively insensitive to the grid resolution provided that both the boundary layers and entrance effects were appropriately resolved. The calculations were performed on workstations, and the CPU times for converged solutions were rather small (e.g., less than ≈1 h) so that high grid densities may be used. The comparison of the results computed for different non-uniform grids ranging from $(M_x = 50 \times M_y = 400)$ to $(M_x = 70 \times M_y = 800)$ showed differences less than 1%. For that reason, a non-uniform grid of (70×600) with stretching parameters $\xi_x = 1.02$ and $\xi_y = 1.007$ in the x- and y-direction, respectively, was used in most of the computations discussed in this study. At the end of each iteration, the residuals for each flow variables were monitored to check the convergence. The convergence criterion required that the scaled residuals be smaller than 10^{-9} for the mass and momentum equations and smaller than 10^{-10} for the energy and species equations.

A comparison with a recently published study by Azizi et al. [22] for small mass flow rates was also carried out. Among the five selected combinations of T_0 and ϕ_0 investigated in [22], two values of the humidity at the inlet section were considered. In both cases, the inlet and wall temperatures were $T_0 = 40\,^\circ C$ and $T_w = 20\,^\circ C$ $(W_{v,w} = 0.0145)$, respectively. The channel aspect ratio was $A = 65$ and the Reynolds number $Re = 300$. The thermophysical properties of humid air were taken to be constant and evaluated by using the 1/3 rule, excepted for reference density and volumetric coefficients of thermal and solutal expansion which were evaluated at the inlet conditions. It is worth noting that the results presented in [22] were obtained, as in Lin et al. [9], by assuming a very low mass fraction of water in the flow field. Therefore, the asymptotic expression of the solutal coefficient of volumetric expansion was used, i.e., $\beta_M = M_a/M_v - 1$. The values of the parameters at the inlet section are given in Table 1. As can be seen, the small values of the buoyancy parameter indicate that thermal buoyancy, acting downward (i.e., in the main flow direction), is largely dominant. In case 1, water is evaporated and the solutal force opposes the flow. On the other hand, vapor is removed from the humid air flow and condensed at the liquid film interface for case 2. Both buoyancy forces act thus in the flow direction. The axial variations of the sensible and latent Nusselt numbers are shown in Fig. 2a and b for the two cases. When assuming constant mixture density evaluated at the inlet temperature, except in the buoyancy

Table 1
Inlet conditions and parameters for validation purpose

T_0 (K)	HR_0 (%)	W_0	ρ_0 (kg m^{-3})	β_T (K^{-1})	β_M	Gr_T	Gr_M	$N = Gr_M/Gr_T$
313	10	0.00456	1.125	0.0032	0.616	−74,576	7142	0.0958
313	50	0.02352	1.112	0.0032	0.584	−74,860	−6123	−0.0818

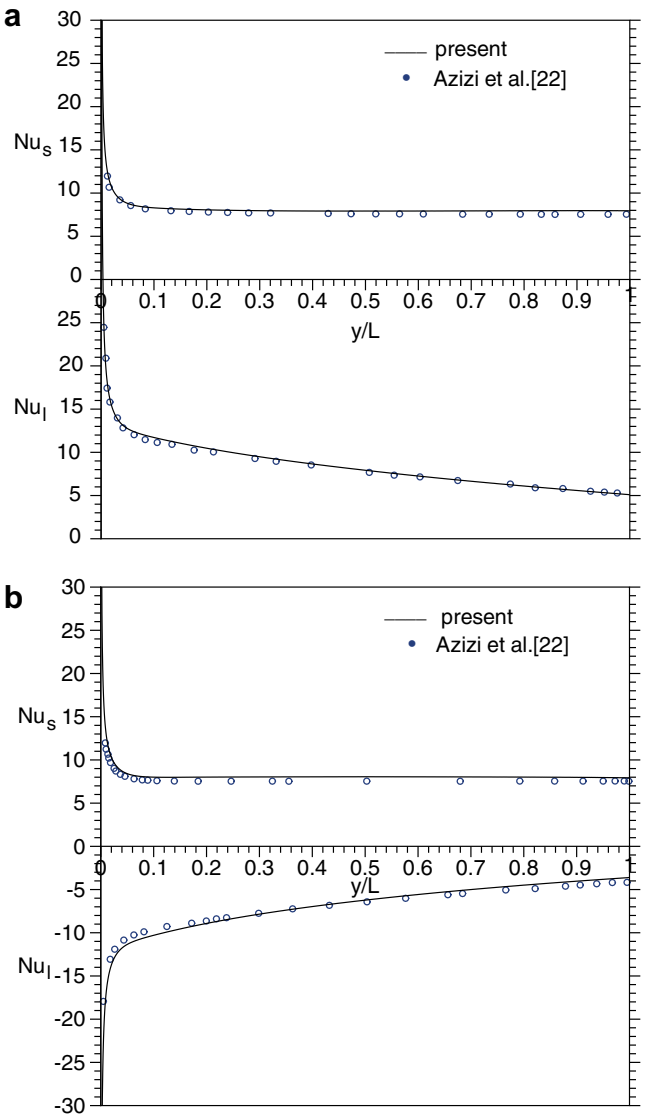

Fig. 2. Comparison of sensible and latent Nusselt number distributions ($T_w = 20\ ^\circ C$, $T_0 = 40\ ^\circ C$, $Re = 300$). (a) $\phi_0 = 10\%$, (b) $\phi_0 = 50\%$.

term, the present results are in excellent agreement with those reported in [22]. When mixture density variations are accounted for, the differences in Nusselt numbers are obviously quite small owing to the low mass flow rates considered.

4. Results and discussion

The calculations were performed for air–water and air–hexane mixtures flowing in a 2-cm wide and 2-m long vertical channel. Dry air entered through the inlet section at uniform downward velocity V_0, ambient temperature T_0 and atmospheric pressure. For water–vapor, the molecular weight of the component ($M_{H_2O} = 18.015$ kg kmol^{-1}) is smaller than that for dry air ($M_a = 28.966$ kg kmol^{-1}) while it is significantly higher for hexane ($M_{C_6H_{14}} = 86.177$ kg kmol^{-1}). Since the analysis is conducted for non-dilute binary mixtures of ideal gases, the results obtained for comparison purposes by invoking the Boussinesq approximation (i.e., $\nabla.\vec{V} = 0$) were based on the following relationship for the density variation in the buoyancy term

$$\rho_m = \rho_0\left(1 - \frac{T - T_0}{T_r} - \frac{(M_a - M_v)W_v}{M_a W_{v,r} + M_v(1 - W_{v,r})}\right) \tag{25}$$

where ρ_0 is the density of ambient dry air ($W_{v,0} = 0$). As for β_T and β_M, the other thermophysical properties were evaluated at the reference temperature T_r and mass fraction $W_{v,r}$ calculated by using the one-third rule [9]

$$T_r = T_w - \frac{1}{3}(T_w - T_0) \quad W_{v,r} = \frac{2}{3}W_{v,w} \tag{26}$$

In the above equation, $W_{v,w}$ is the vapor mass fraction at saturation conditions given by Eq. (11). By assuming constant thermophysical properties and Boussinesq approximation, mixed convection heat and mass transfer depends on the dimensionless parameters Re_0, Gr_T, Gr_M, Pr, Sc and A. Since they are interdependent for a given mixture, the Reynolds number at the inlet section, the channel aspect ratio and the interfacial mass fraction were the only dimensionless parameters which were arbitrarily assigned. The others were calculated under specific conditions for which all the mixture properties used for the computations are reported in the following sections.

4.1. Evaporation of water into air stream

4.1.1. Solutal mixed convection

A first series of computations was carried out with the incoming dry air temperature at the inlet equal to the wall temperature ($T_0 = T_w$). Therefore, the buoyancy term in the y-momentum equation is only due to solutal effects ($\rho_m = \rho_m(W_v)$ and $Gr_T = 0$). Five values of the interfacial mass fraction of water vapor ranging from $W_{v,w} = 0.1$ to $W_{v,w} = 0.5$ were considered. The inlet Reynolds number was assigned 300, 600 or 900 and the channel aspect ratio $A = 100$. In order to examine the specific effect of density variation thoroughly, the other thermophysical properties are taken to be constant and evaluated by using the one-third rule. Since the hydraulic diameter is chosen to be $D_h = 4$ cm, all the thermophysical properties are deduced from a given set (T_0, Re_0, $W_{v,w}$) according to the formulae used for calculating the properties of dry air, water vapor and their mixture. In the present study, we used the correlations given by Fujii et al. [23]. The data reported in Table 2 were thus employed for computations based either on Boussinesq approximation or variable mixture density. Table 2 shows the increases in the solutal Grashof and Richardson numbers, $Ri_M = Gr_M/Re_0^2$, as the interfacial vapor mass fraction increases. Since the solutal force is in the upward direction, flow reversal may thus occur at the largest $W_{v,w}$-values for which Ri_M becomes much larger than unity.

The development of the axial velocity component is shown in Fig. 3 for $W_{v,w} = 0.1$ and $W_{v,w} = 0.5$ at $Re_0 = 300$. Very close to the channel entrance, a flat velocity profile is seen in the core region because the buoyancy effects are weak. As the flow goes downstream, evaporation produces a significant increase in axial velocity at the core region in comparison with pure forced flow at $Re_0 = 300$. The velocity profiles develop gradually from distorted

Table 2
Thermophysical properties of air–water vapor mixture based on the 1/3-rule (except density) and dimensionless parameters for various interfacial mass fractions of water vapor ($Re = 300$)

Case	$W_{v,w}$	$T_w = T_0$ (K)	ρ_0 (kg m^{-3})	μ_t (kg m^{-1} s^{-1})	β_M	D_{v,m_t} (m^2 s^{-1})	Gr_M	Sc	Ri_M
1	0.1	327.5	1.077	1.874×10^{-5}	0.584	3.290×10^{-5}	1.212×10^{5}	0.529	1.346
2	0.2	341.5	1.034	1.841×10^{-5}	0.562	3.553×10^{-5}	1.225×10^{5}	0.501	1.361
3	0.3	349.8	1.009	1.790×10^{-5}	0.542	3.713×10^{-5}	3.244×10^{5}	0.477	3.604
4	0.4	355.5	0.993	1.735×10^{-5}	0.523	3.824×10^{-5}	4.303×10^{5}	0.457	4.781
5	0.5	360	0.980	1.678×10^{-5}	0.505	3.913×10^{-5}	5.407×10^{5}	0.438	6.008

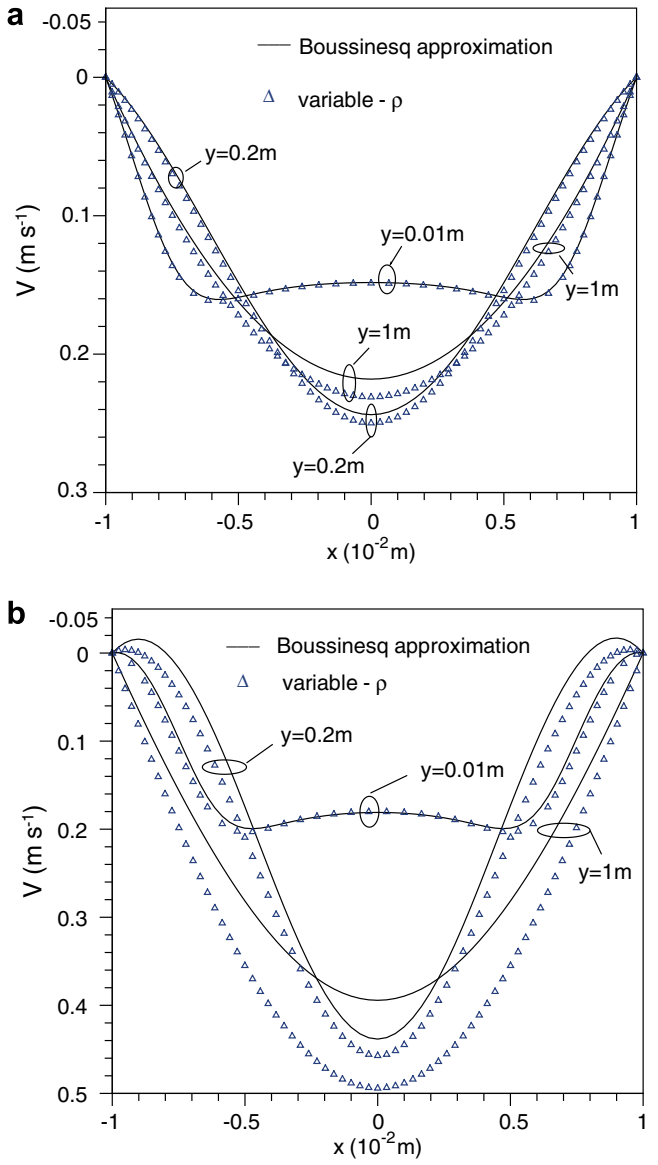

Fig. 3. Vertical velocity profiles for $Re = 300$. (a) $W_{v,w} = 0.1$, (b) $W_{v,w} = 0.5$.

profiles to parabolic ones in the fully developed regime where a pure Poiseuille flow is recovered owing to the large channel aspect ratio, Schmidt number and low Reynolds number values. For $W_{v,w}$ larger than ≈0.2, upward velocities are observed in the wall regions due to stronger solutal buoyancy forces near the wetted surfaces. As a result, the flow acceleration in the core region is greater for large mass evaporation rates. Fig. 4 shows axial velocity isocontours (left-hand side) together with streamlines (right-hand side) over the whole channel length (the channel width being expanded for clarity) for cases 1, 2 and 5 depicted in Table 2. Due to the perfect symmetry of the flow fields computed within the present study, these plots are restricted to one half of the channel section. The cells centered at the channel axis correspond to maximal downward velocities while the two cells attached to the wetted walls in the entrance region are for upward axial velocities, as can be clearly seen from the streamlines for case 5 (Fig. 4c).

For case 1 (Fig. 4a), the flow is downward at every channel location due to the small local value of the Richardson number (i.e., based on the local difference between wall and bulk mass fractions). Fig. 3 allows also comparisons between velocity profiles based either on Boussinesq or variable density formulations. The differences in the velocity for the two cases increase as the interfacial mass fraction is augmented and in the fully developed region where maximum effects caused by the decrease in mixture density occur. The explanation is that moist air is then at saturation conditions owing to the low Re-value considered. It should be noted that the solutal effects do not greatly modify the developing length because the Schmidt number is less than unity (i.e., the dynamical entry length is larger than the solutal entry length).

The axial variations of the bulk mixture density are displayed in Fig. 5 according to the $W_{v,w}$-value. The decrease in $\bar{\rho}_m$ is obviously greater for larger evaporation rates of liquid water, the differences between the inlet and outlet mixture density being from 4% to 25% when increasing $W_{v,w}$ from 0.1 to 0.5. Therefore, the Boussinesq approximation is not valid from a theoretical point of view when the change in mass fraction of water vapor between inlet and outlet sections exceeds about $\Delta W_v = 0.2$. However, the overall effect of this approximation is rather small when considering the mass flow rate at the outlet section (Fig. 6). As expected, these results imply that the mass fraction profiles become independent of the problem formulation as the flow proceeds downstream. The differences between the interfacial and bulk mass fractions of water vapor do indeed decrease while the flow is developing. Finally, the vaporization rate vanishes in the fully developed regime and a pure forced flow is predicted.

Inspection of the mass fraction conservation equation readily reveals that the influence of density variations is closely related to the relative importance of convective terms to diffusive terms. Therefore, an increase in the inlet Reynolds number leads to opposite effects under given specific conditions: a decrease in the solutal Richardson number and an increase in the effects of density variations in the transport terms for both momentum and mass fraction equations. The reduction in the relative importance of the solutal buoyancy force leads to the disappearance of upward axial velocities in the entrance region for the highest $W_{v,w}$-value considered, as displayed in Fig. 7 for $Re_0 = 900$ and $W_{v,w} = 0.5$. Small relative differences between Boussinesq and variable density formulations are however predicted. On the other hand, Fig. 8 shows significant increases in the effects of mixture density variations on the vaporized mass flow rate when increasing the inlet Reynolds number, the differences between interfacial and axial water–vapor mass fraction increase with Re_0 at any selected cross-section. The main reasons are the increases in both the developing length and relative importance of the transport terms in the mass fraction conservation equation. As a result, the discrepancies

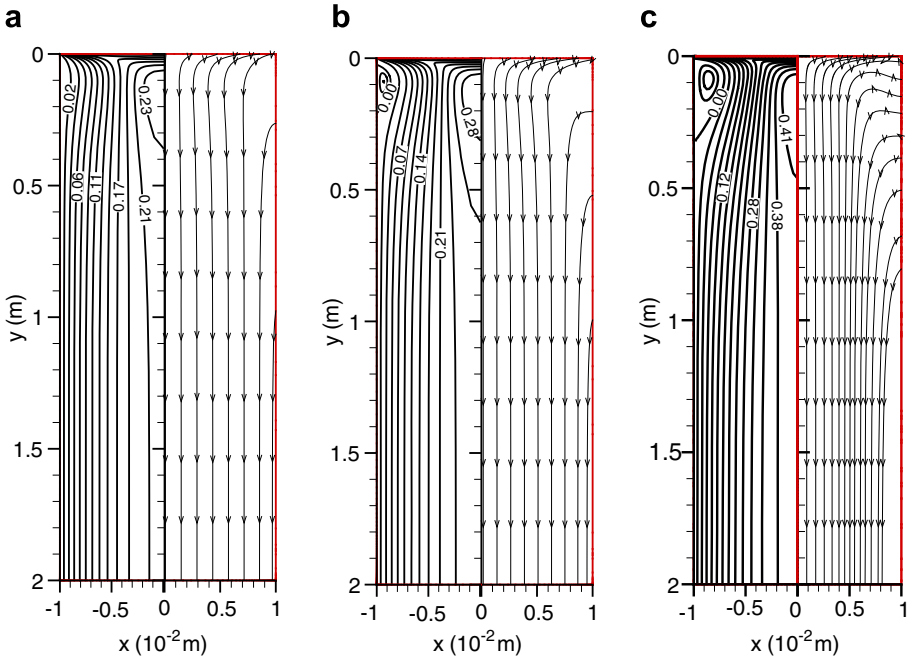

Fig. 4. Isolines of vertical velocity and streamlines for $Re = 300$. (a) $W_{v,w} = 0.1$ and $\psi_{max} = 3.12 \times 10^{-3}$ kg m^{-1} s^{-1}, (b) $W_{v,w} = 0.2$ and $\psi_{max} = 3.45 \times 10^{-3}$ kg m^{-1} s^{-1}, (c) $W_{v,w} = 0.5$ and $\psi_{max} = 5.07 \times 10^{-3}$ kg m^{-1} s^{-1} with $\Delta\psi \approx 3.90 \times 10^{-4}$ kg m^{-1} s^{-1}.

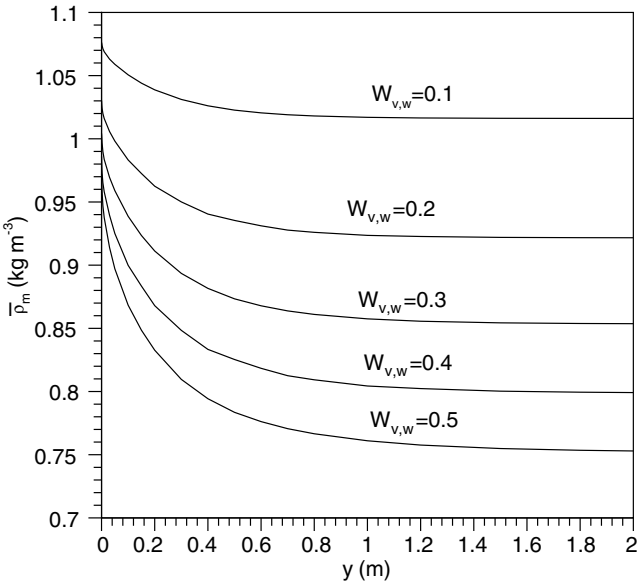

Fig. 5. Bulk mixture density variation for various interfacial mass fractions of water vapor and $Re = 300$.

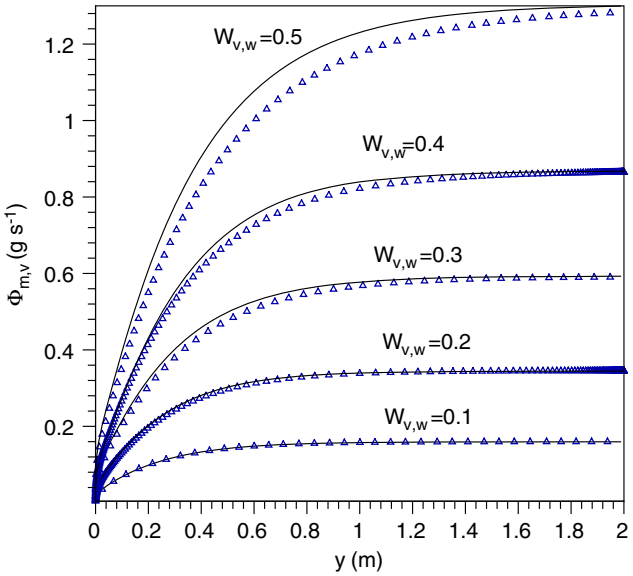

Fig. 6. Vaporized mass flux rate variations for various interfacial mass fractions of water vapor and $Re = 300$ (—, Boussinesq approximation; △ variable-ρ).

between the mass flow rate of vaporized water at the outlet section are larger as shown in Fig. 8.

4.1.2. Thermosolutal mixed convection

In order to examine thermal effects on the previous results, a number of computations were carried out for various combinations of inlet and wall temperatures. When $T_0 \geqslant T_w$, vaporization occurs with the thermal buoyancy force opposing the solutal force in the case of liquid water evaporation. Amongst the calculations carried out, only the two cases for inlet Reynolds numbers $Re_0 = 300$ and 600 are discussed here. The other selected parameters reported in Table 3 are for an inlet dry air temperature $T_0 = 370$ K and wall temperature $T_w = 349.8$ K which yields an interfacial water–vapor mass fraction $W_{v,w} = 0.3$. From the thermophysical properties reported in Table 3, the values of the Grashof numbers for heat and mass transfer are $Gr_T = -9.76 \times 10^4$ and $Gr_M = 2.80 \times 10^5$. The buoyancy parameter being $N = -2.87$, the solutal forces are thus dominant. Since $Gr_T + Gr_M > 0$, the combined buoyancy forces act in the upward direction. In this section, the thermophysical properties (except density) were calculated according to the 1/3 rule.

The channel length at which the developed velocity profiles for pure forced flow are reached within 1% is slightly larger than $A/2$ (half of the channel height) for $Re_0 = 300$ and close to $2A/3$ for $Re_0 = 600$. This result shows that the effective Grashof numbers (i.e., Gr_T and Gr_M based on local differences between wall and bulk

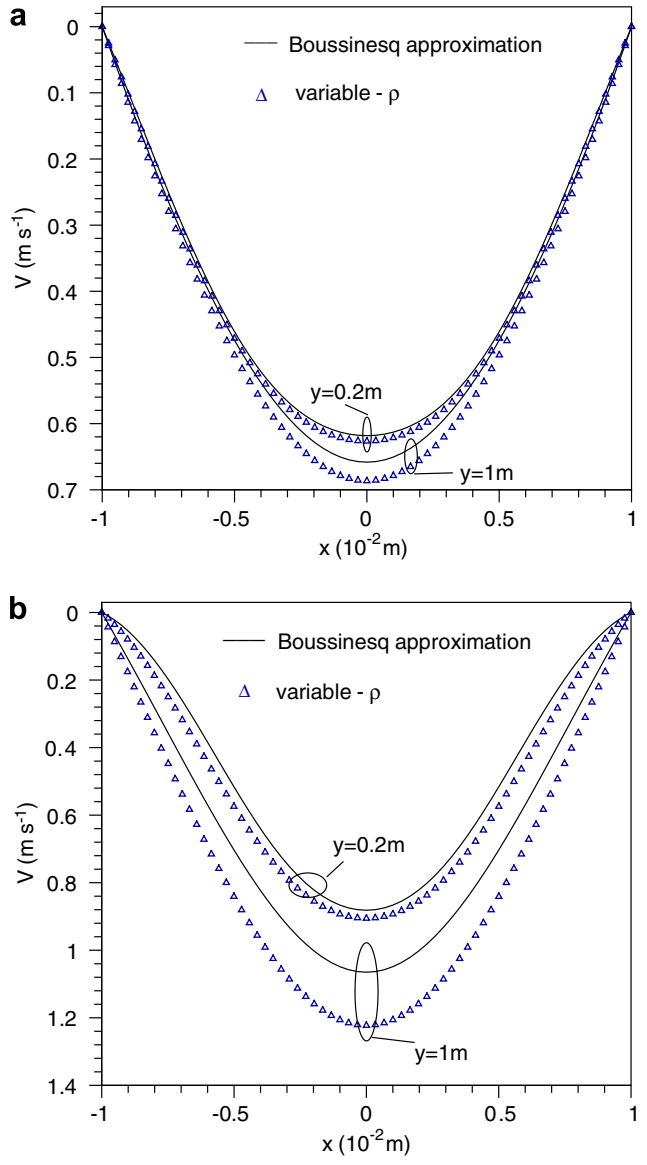

Fig. 7. Vertical velocity profiles for solutal mixed convection of air–water vapor mixture and $Re = 900$. (a) $W_{v,w} = 0.1$, (b) $W_{v,w} = 0.5$.

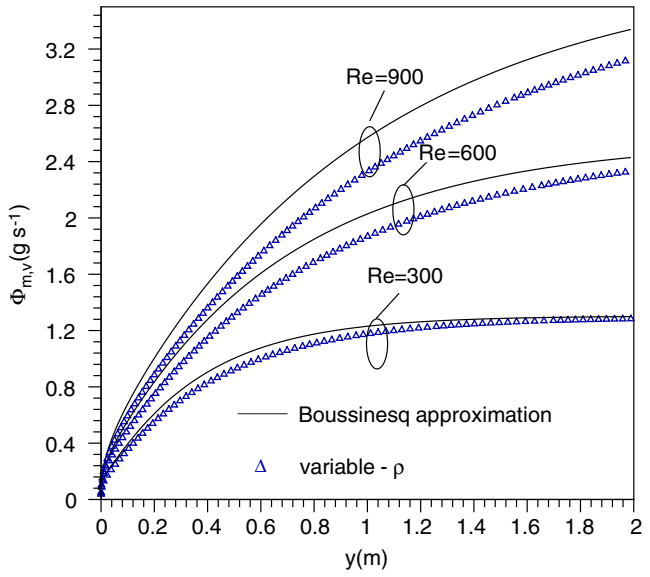

Fig. 8. Variations of vaporized mass flux rate of liquid water for various inlet Reynolds numbers and $W_{v,w} = 0.5$ (—, Boussinesq approximation, △ variable-ρ).

temperature and mass fraction) become very small. In comparison with the isothermal case, the main changes in the velocity profiles are observed near the channel inlet where the combination of external force and thermal buoyancy force is enough to suppress the reversal flows close to the walls at $Re_0 = 300$, as can be seen in Fig. 9 showing the downward velocity isocontours (left-hand side) and streamlines (right-hand side). Therefore the maximum axial velocity increases continuously as the humid air proceeds downstream. However, since the Boussinesq approximation can be invoked for the thermal part of the problem owing to the small temperature difference $(T_0 - T_w)$ and opposing thermal and solutal forces, the effects of water vaporization on the mixture mass fraction field are less than for isothermal flows. At the channel outlet, the average velocity and mixture density are $\overline{V} = 0.45$ m/s and $\bar{\rho}_m = 0.854$ kg/m^3 when mixture density variations are accounted for in the case $Re_0 = 600$, that is to say an increase in velocity and a decrease in density of about 10% in comparison with the Boussinesq formulation. On the other hand, the bulk temperature and mass flow rate of vaporized water are much less dependent on the problem formulation. Fig. 10 illustrates the development of temperature at selected channel cross-sections for the two inlet Reynolds numbers for which the global Richardson numbers at the inlet section $(Gr_T + Gr_M)/Re_0^2$ are $Ri = 2.02$ and $Ri = 0.5$. When increasing Re, the thermal and solutal developing lengths increase as well as the mass fraction and temperature gradients at the walls. Both temperature and mass fraction develop similarly but the growth in thickness of the temperature boundary layers is a little slower than those of the solutal ones because the Prandtl number is higher than the Schmidt number ($Pr = 0.73$, $Sc = 0.50$). For the two Re-values, the average temperature and mass fraction at the outlet section are very close to T_p and $W_{v,w}$. Therefore, the flow can be assumed as fully developed at the channel end region.

It is of interest to examine the effects of liquid film vaporization on the distributions of sensible and latent heat flux densities at the walls, q_l/q_s. Fig. 11 shows first that heat transfer due to latent heat exchange is much more effective, especially in the developing region. Second, a sharp decrease in the ratio of local latent heat flux to sensible heat flux is displayed in Fig. 11 because water evaporates faster in dry air than in moist air. In the entrance region, the temperature potential change $(\overline{T}_m(y) - T_w)$ is less than the mass fraction potential change owing to the difference between Pr and Sc. Also found in this figure is the effect of Re on the variation of q_l/q_s: a higher heat transfer enhancement due to film evaporation is seen for a flow with a larger Re. It should be noted that these overall trends are the same for both Boussinesq and variable density formulations.

4.2. Evaporation of hexane into air stream

The channel aspect ratio and Reynolds number at the inlet section were assigned $A = 100$ and $Re = 300$, respectively. The temperature-dependent properties of hexane were calculated by employing the algebraic forms given in Lide and Kehiaian [24]. In all of the cases investigated, dry air entered through the inlet section and the mixture was considered as a binary ideal gas with the mass diffusion coefficient calculated by using the Chapman–Enskog formula, and the dynamic viscosity and thermal conductivity by Wilke's formulae [25]. The property calculations for the mixture were quite complex and it is believed that the thermophysical values reported in the Tables presented in this section are the best presently available [24].

Table 3
Values of parameters for thermosolutal mixed convection of air–water vapor mixture based on the 1/3-rule ($T_0 = 370$ K, $T_w = 349.8$ K, $h_{lg} = 2.317 \times 10^6$ J kg^{-1})

$W_{v,w}$	ρ_0 (kg m^{-3})	k_r (W m^{-1} K^{-1})	$C_{p,r}$ (J kg^{-1} K^{-1})	μ_r (kg m^{-1} s^{-1})	β_T (K^{-1})	β_M	D_{v,m_r} (m^2 s^{-1})	Pr	Sc
0.3	0.954	0.030	1202	1.820×10^{-5}	0.0028	0.542	3.844×10^{-5}	0.725	0.496

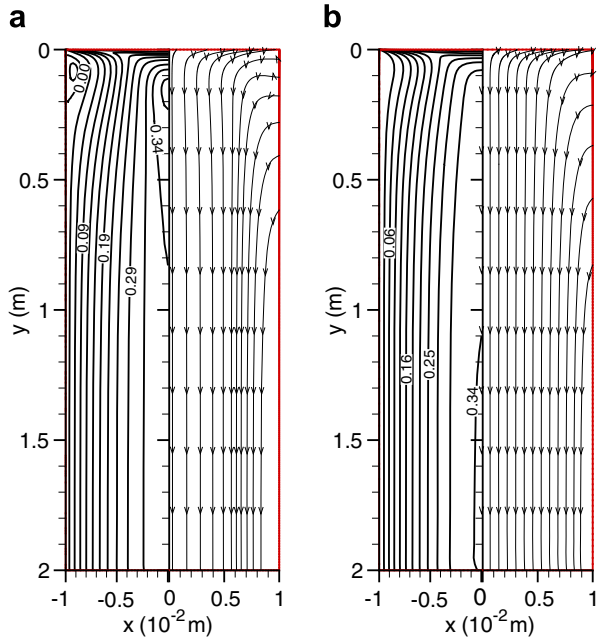

Fig. 9. Isolines of vertical velocity and streamlines for $Re = 300$ and $W_{v,w} = 0.3$. (a) $T_0 = T_w = 349.8$ K and $\psi_{max} = 3.86 \times 10^{-3}$ kg m^{-1} s^{-1}, (b) $T_0 = 370$ K, $T_w = 349.8$ K and $\psi_{max} = 3.94 \times 10^{-3}$ kg m^{-1} s^{-1} with $\Delta\psi \approx 3.03 \times 10^{-4}$ kg m^{-1} s^{-1}.

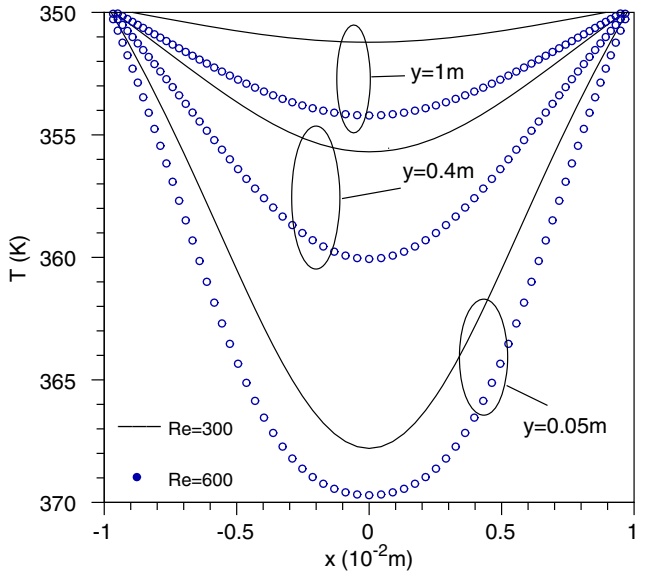

Fig. 10. Comparison between temperature profiles for thermosolutal mixed convection of air–water vapor mixture ($W_{v,w} = 0.3$, $T_0 = 370$ K, $T_w = 349.8$ K).

4.2.1. Solutal mixed convection

Five values of the interfacial mass fraction of hexane vapor ranging from $W_{v,w} = 0.1$ to $W_{v,w} = 0.5$ were considered. The corresponding thermophysical properties and dimensionless parameters calculated by using the 1/3 rule are reported in Table 4. For air–hexane mixture, the solutal coefficient of volumetric expansion

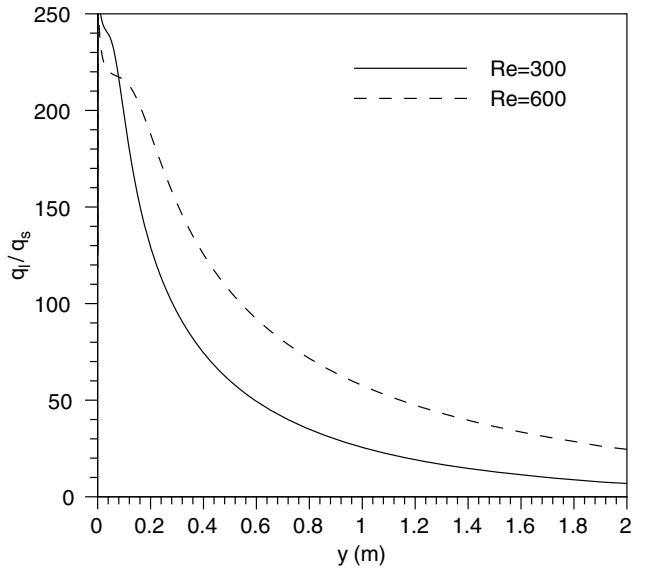

Fig. 11. Axial variation of the latent to sensible heat flux ratio for thermosolutal mixed convection of air–water vapor mixture ($W_{v,w} = 0.3$, $T_0 = 370$ K, $T_w = 349.8$ K).

being negative, the buoyancy force acts downward when dry air enters the channel and the mixture density is much larger close to the walls than in the channel core, especially in the entrance region. Therefore, mass diffusion produces both a strong flow acceleration in the solutal boundary layers, as shown in Fig. 12 for $W_{v,w} = 0.5$, and flow recirculations at the channel center where upward velocities are predicted as can be seen at section $y = 0.15$ m. The flow is thus always downward near the solid walls and the size and onset of the cells which occur near the inlet section depends on the vaporization rate (i.e., the assigned value of $W_{v,w}$). Fig. 12 shows that upward axial velocities are damped as the fluid proceeds downward. A velocity profile with a maximal velocity located at the channel axis is gradually recovered at distances from the inlet section much larger than in the case of water evaporation owing to the larger Schmidt number value ($Sc = 1.55$). For the highest $W_{v,w}$-value considered in the present study, Fig. 12 indicates clearly that the fully developed regime is not reached at the channel outlet section.

The plots of the isovalues of the axial velocity displayed in Fig. 13 (left-hand side) provide a better insight into the nature of the flow field, which exhibits features opposite to those observed in the case of evaporation of liquid water films: the center of the closed isolines located near the left (or right) walls and inlet section shows the locus of the point where $v(x, y)$ is maximum; the closed isoline adjacent to the channel centerline having a zero value determines the boundary of the region where the axial velocity is upward. The streamlines presented at the right-hand side of Fig. 13 reveal the onset of flow recirculations at the channel core region for $W_{v,w} \geqslant 0.2$. This is a direct consequence of the larger solutal buoyancy effect as $W_{v,w}$ is increased owing to the large introduction of hexane vapor into the channel. Fig. 13 shows also that the extent of the boundary layer region in which the peak in downward velocity occurs is progressively increased as the interfacial mass fraction is augmented.

Table 4
Thermophysical properties of air–hexane mixture based on the 1/3-rule (except density) for various interfacial mass fractions of hexane vapor

$W_{v,w}$	$T_w = T_0$ (K)	ρ_0 (kg m^{-3})	μ_r (kg m^{-1} s^{-1})	β_M	D_{v,m_r} (m^2 s^{-1})	Gr_M	Sc
0.1	264	1.337	1.593×10^{-5}	−0.694	6.098×10^{-6}	-4.42×10^5	1.95
0.2	278	1.269	1.579×10^{-5}	−0.728	6.733×10^{-6}	-5.90×10^5	1.85
0.3	288	1.226	1.540×10^{-5}	−0.765	7.195×10^{-6}	-9.13×10^5	1.74
0.4	296	1.192	1.492×10^{-5}	−0.806	7.587×10^{-6}	-12.9×10^5	1.65
0.5	304	1.163	1.437×10^{-5}	−0.852	7.949×10^{-6}	-17.5×10^5	1.55

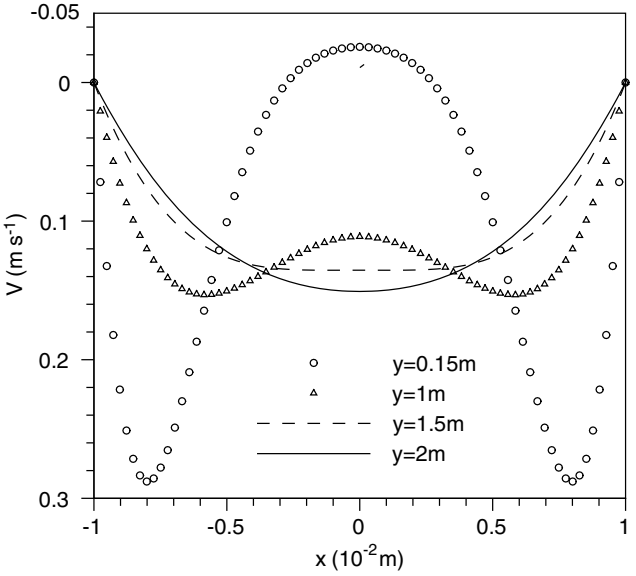

Fig. 12. Vertical velocity profiles for solutal mixed convection of air–hexane mixture ($Re = 300$, $W_{v,w} = 0.5$).

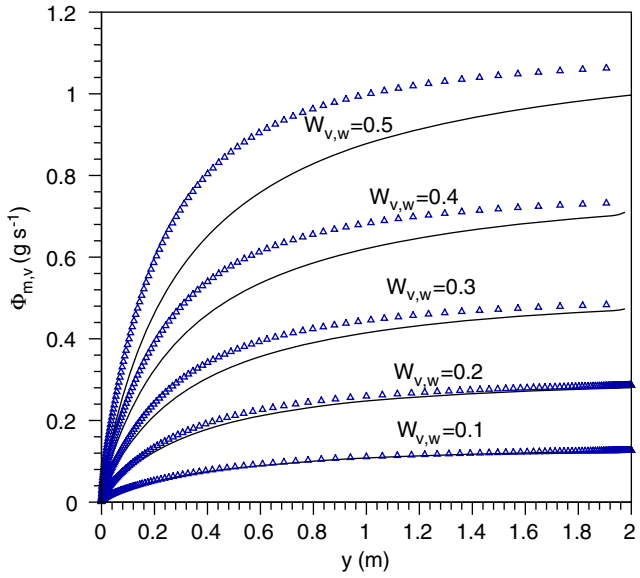

Fig. 14. Effects of interfacial mass fraction on vaporized mass flux distribution for solutal mixed convection of air–hexane mixtures and $Re = 300$ (—, Boussinesq approximation, △ variable-ρ).

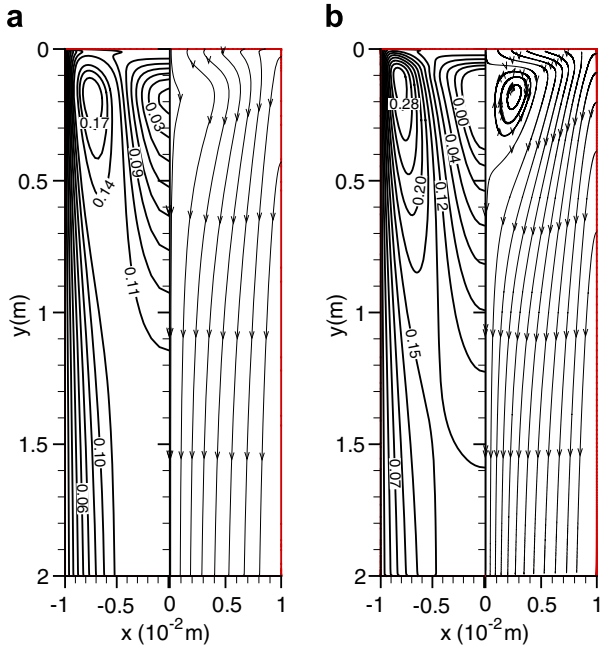

Fig. 13. Isolines of vertical velocity and streamlines for solutal mixed convection of air–hexane mixture and $Re = 300$. (a) $W_{v,w} = 0.2$ and $\psi_{max} = 2.94 \times 10^{-3}$ kg m^{-1} s^{-1}, (b) $W_{v,w} = 0.5$ and $\psi_{max} = 4.28 \times 10^{-3}$ kg m^{-1} s^{-1} with $\Delta\psi \approx 3.28 \times 10^{-4}$ kg m^{-1} s^{-1}.

The influences of $W_{v,w}$ on the mass flow rate entering into the air stream from one of the wetted walls are presented in Fig. 14 for Boussinesq and variable density formulations. The overall tendency is similar to what was found for water vaporization and identical interfacial mass fraction (see Fig. 6). However, it is seen first that a smaller liquid vaporization is experienced because the mass diffusion coefficient is about 6 times smaller for hexane than for water. Secondly, the axial variation of the evaporation rate shows that the average mass fraction at the channel outlet section has not yet reached the interfacial value, especially for the highest $W_{v,w}$-values considered. It is also clear that the discrepancies between the Boussinesq and variable density formulations are significantly augmented as $W_{v,w}$ is increased. The largest differences are observed in the developing region because the mixture tends to be saturated as the fluid proceeds downward, whatever the formulation employed.

4.2.2. Thermosolutal mixed convection

The computations were carried out for dry air entering at $T_0 = 333$ K and for an interfacial film temperature $T_w = 288$ K. Since the thermophysical properties of an air–vapor hexane mixture vary significantly with both temperature and mass fraction, comparison between the results obtained by assuming constant properties (except density) and variable properties are discussed in this section. The corresponding thermophysical properties and dimensionless parameters calculated by using the 1/3 rule are reported in Table 5. Based on these data, the magnitudes of the thermal and solutal Grashof numbers are of the same order of magnitude: $Gr_T = -4.08 \times 10^5$ and $Gr_M = -6.30 \times 10^5$.

Fig. 15 shows the development of the streamwise velocity profile for solutal (i.e., $T_0 = T_w = 288$ K) and thermosolutal conditions. The fluid near the channel walls is accelerated by the buoyancy force and its velocities are thus greater than the corresponding

Table 5
Values of parameters for thermosolutal mixed convection of air–hexane vapor mixture based on the 1/3-rule ($T_0 = 333$ K, $T_w = 288$ K, $h_{lg} = 0.3614 \times 10^6$ J kg^{-1})

ρ_0 (kg/m^3)	$W_{v,w}$	k_r (W m^{-1} K^{-1})	$C_{p,r}$ (J kg^{-1} K^{-1})	μ_r (kg m^{-1} s^{-1})	β_T (K^{-1})	β_M	D_{v,m_r} (m^2 s^{-1})	Pr	Sc
1.060	0.3	0.0235	1140	1.603×10^{-5}	0.0033	−0.765	7.919×10^{-6}	0.778	1.909

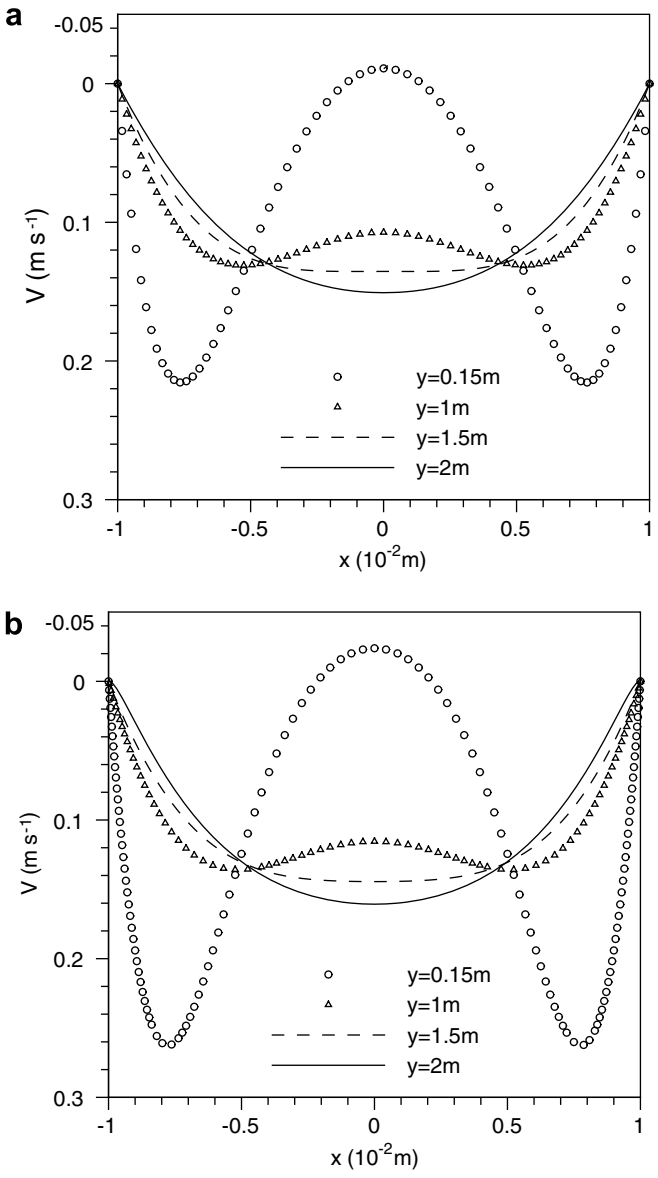

Fig. 15. Vertical velocity profiles for air–hexane mixture ($Re = 300$, $W_{v,w} = 0.3$). (a) Solutal mixed convection, (b) thermosolutal mixed convection.

ones for solutal convection. Therefore, the opposite is displayed in the core region as a consequence of mass conservation. It should be noted that the differences between solutal and thermosolutal profiles are more pronounced for lower interfacial mass fractions owing to the decrease in the buoyancy parameter, $N = Gr_M/Gr_T$. The general flow features are presented in Fig. 16 for solutal and thermosolutal flows. Since both buoyancy forces are aiding, the thermal buoyancy force produces larger extents of the regions of maximum streamwise velocity adjacent to the walls and of the recirculating cells in the channel core.

Finally, the effects of variations of all thermophysical properties with mixture temperature and mass fraction of hexane vapor were accounted for. It should be emphasized that the results discussed here are linked to the specific conditions applied. The changes in the thermophysical properties of the mixture with mass fraction and temperature are indeed different: according to the Chapman–Enskog relationship, the mass diffusion coefficient for a binary mixture does not depend on the mass fraction, and decreases with temperature; mixture density increases in the downward direction, since temperature decreases and the mass fraction of hexane increases; both dynamic viscosity and thermal conductivity decrease as the mass fraction is augmented and temperature is reduced, and mass fraction and temperature have opposite effects on specific heat. The overall results are summarized by the plots of streamwise variations of the normalized thermophysical properties along the channel centerline as shown in Fig. 17. As can be seen, the increase in mixture density is as much as 40% between the inlet and outlet sections, while the decreases in dynamic viscosity, thermal conductivity and mass diffusion coefficient are about 25%. The combined effects of these thermophysical properties variations on the Prandtl number are rather small but quite large on the Schmidt number. However, Fig. 17 shows that the changes in the thermophysical properties are significant in the entrance region only, i.e., where the gradients in mass fraction and temperature are the largest. As a result, velocity and temperature fields are mostly influenced by thermophysical property variations in the first half of the channel length. Comparisons between Fig. 16b and c assess this prediction. The results showed that temperature is the flow variable the most influenced by variations of the thermophysical properties. However, Fig. 18 shows that such effects are restricted to the first half length of the channel.

5. Conclusions

The effect of buoyancy forces, assisting or opposing, on developing mixed thermosolutal convection between vertical plates has been numerically simulated by using a non-Boussinesq formulation. Entrance flow effects and variable thermophysical properties have been numerically investigated. Results are presented for a duct with an aspect ratio $A = 100$ at various Reynolds numbers. Evaporations of water and hexane liquid films were considered for various interfacial mass fractions and wall-to-inlet temperature differences. In the first case, the solutal buoyancy force acts in the upward direction. For hot dry air entering into the channel with a flat velocity profile through the top cross-section, the thermal and solutal forces are opposing. For hexane evaporation, the solutal force acts downward. The buoyancy forces are thus aiding and act in the direction of the external force. Therefore, the overall features of the flow field differ considerably for evaporation of these two liquid films. In the case of water evaporation at constant temperature, the maximum downward velocities predicted at the channel core in the entrance region are much larger than for forced convection. Large mass diffusion fluxes near the wetted walls due to the solutal potential may produce upward velocities in the boundary layers according to the value of the interfacial mass fraction. This is a result of large changes in the mixture density profiles in the entrance region. Such flow reversal cannot occur when the dilute binary mixture assumption is invoked. On the other hand, evaporation of a component heavier than the carrier gas leads to flow acceleration in the boundary layers. When the interfacial mass fraction is large enough ($W_{v,w} \geqslant 0.2$ for air–hexane system), flow recirculations are predicted at the channel center. The size of

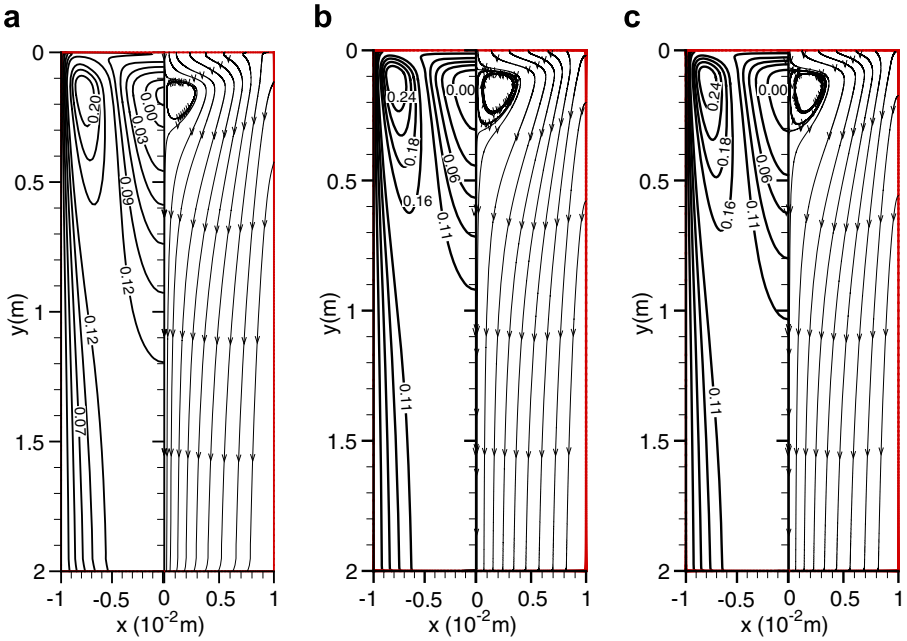

Fig. 16. Isolines of vertical velocity and streamlines for mixed convection of air–hexane mixture, $Re = 300$ and $W_{v,w} = 0.3$. (a) Isothermal flow ($\psi_{max} = 3.28 \times 10^{-3}$ kg m^{-1} s^{-1}), (b) thermosolutal flow with constant thermophysical properties (except ρ) ($\psi_{max} = 3.42 \times 10^{-3}$ kg m^{-1} s^{-1}), (c) thermosolutal flow with all thermophysical properties varying with temperature and mass fraction ($\psi_{max} = 3.41 \times 10^{-3}$ kg m^{-1} s^{-1}).

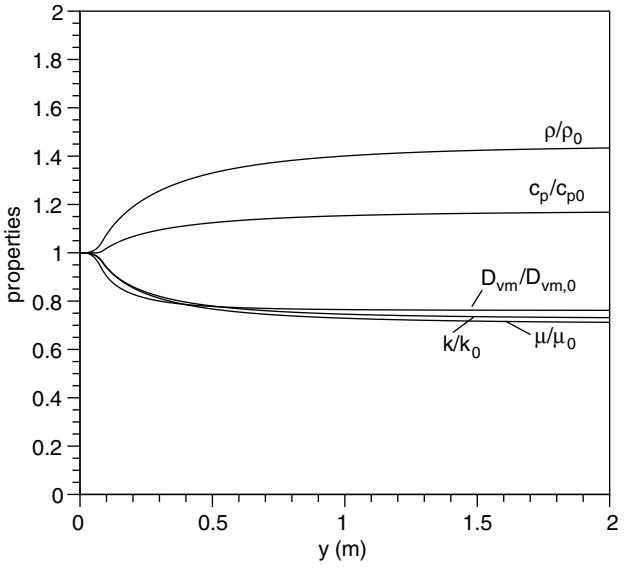

Fig. 17. Axial variations of the centerline thermophysical properties of hexane normalized by the inlet values ($W_{v,w} = 0,3$, $T_0 = 333$ K, $T_w = 288$ K).

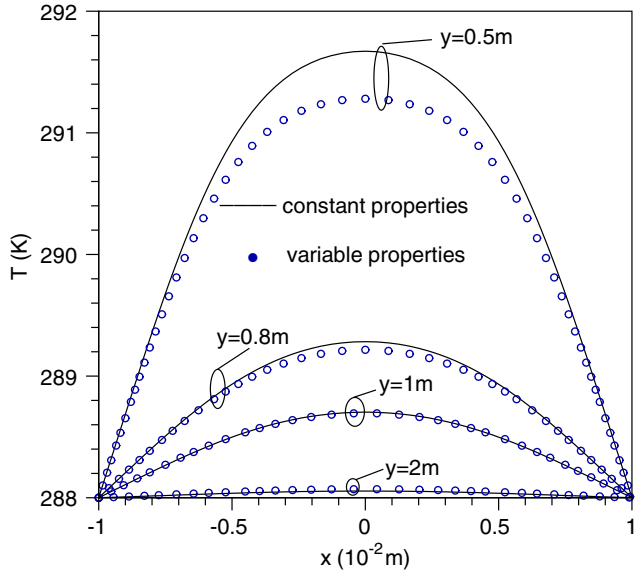

Fig. 18. Temperature profiles at various sections for thermosolutal mixed convection: effects of variations of all mixture thermophysical properties with temperature and mass fraction (hexane, $Re = 300$, $W_{v,w} = 0,3$, $T_0 = 333$ K, $T_w = 288$ K).

the recirculation cell increases as the interfacial mass fraction increases. When using a parabolic flow formulation, as has been done in most of the studies published in the archival literature, this flow structure cannot be predicted. In addition, the influence of variations of all the mixture thermophysical properties on the flow field may be important, especially for thermosolutal mixed convection.

References

[1] E.V. Somers, Theoretical considerations of combined thermal and mass transfer from a vertical plate, J. Appl. Mech. 23 (1956) 295–301.
[2] H. Nakamura, Bull. Jpn. Soc. Mech. Eng. 5 (1962) 311.
[3] L.C. Chow, J.N. Chung, Evaporation of water into a laminar stream of air and superheated steam, Int. J. Heat Mass Transf. 26 (1983) 373–380.
[4] E.M. Sparrow, J.L. Gregg, The variable fluid-property problem in free convection, Trans. Am. Soc. Mech. Eng. 80 (1958) 879–886.
[5] M. Haji, L.C. Chow, Experimental measurement of water evaporation rates into air and superheated steam, ASME J. Heat Transf. 110 (1988) 237–242.
[6] T.S. Lee, P.G. Parikh, A. Acrivos, D. Bershader, Natural convection in a vertical channel with opposing buoyancy forces, Int. J. Heat Mass Transf. 25 (1982) 499–511.
[7] C.J. Chang, T.F. Lin, W.M. Yan, Natural convection flows in a vertical, open tube resulting from combined buoyancy effects on thermal and mass diffusion, Int. J. Heat Mass Transf. 29 (1986) 1543–1552.
[8] W.M. Yan, T.F. Lin, Effects of wetted wall on laminar mixed convection in a vertical channel, J. Thermophys. 3 (1989) 94–96.
[9] T.F. Lin, C.J. Chang, W.M. Yan, Analysis of combined buoyancy effects of thermal and mass diffusion on laminar forced convection heat transfer in a vertical tube, ASME J. Heat Transf. 110 (1988) 337–344.

[10] W.M. Yan, Mixed convection heat transfer enhancement through latent heat transport in vertical parallel plate channel flows, Can. J. Chem. Eng. 69 (1991) 1277–1282.
[11] W.M. Yan, Y.L. Tsay, T.F. Lin, Simultaneous heat and mass transfer in laminar mixed convection flows between vertical plates with asymmetric heating, Int. J. Heat Fluid Flow 10 (1989) 262–269.
[12] Y.L. Tsay, T.F. Lin, Combined heat and mass transfer in laminar gas stream flowing over an evaporating liquid film, Wärme und Stoffübertragung 25 (1990) 213–221.
[13] W.M. Yan, T.F. Lin, Combined heat and mass transfer in natural convection between vertical plates with film evaporation, Int. J. Heat Mass Transf. 33 (1990) 529–541.
[14] W.M. Yan, The effect of liquid film vaporization on natural convection heat and mass transfer in a vertical tube, Can. J. Chem. Eng. 70 (1992) 452–462.
[15] W.M. Yan, Effects of film evaporation on laminar mixed convection heat and mass transfer in a vertical channel, Int. J. Heat Mass Transf. 35 (1992) 3419–3429.
[16] J.H. Jang, W.M. Yan, Thermal protection with liquid film in turbulent mixed convection channel flows, Int. J. Heat Mass Transf. 49 (2006) 3645–3654.
[17] K.T. Lee, H.L. Tsai, W.M. Yan, Mixed convection heat and mass transfer in vertical rectangular ducts, Int. J. Heat Mass Transf. 40 (1997) 1621–1631.
[18] C.C. Huang, W.M. Yan, J.H. Jang, Laminar mixed convection heat and mass transfer in vertical rectangular ducts with film evaporation and condensation, Int. J. Heat Mass Transf. 48 (2005) 1772–1784.
[19] J.H. Jang, W.M. Yan, C.C. Huang, Mixed convection heat transfer enhancement through film evaporation in inclined square ducts, Int. J. Heat Mass Transf. 48 (2005) 2117–2125.
[20] G. Desrayaud, G. Lauriat, Heat and mass transfer analogy for condensation of humid air in a vertical channel, Heat Mass Transf. 37 (2001) 67–76.
[21] Z.A. Hammou, B. Benhamou, N. Galanis, J. Orfi, Laminar mixed convection of humid air in a vertical channel with evaporation or condensation at the wall, Int. J. Therm. Sci. 43 (2004) 531–539.
[22] Y. Azizi, B. Benhamou, N. Galanis, M. El-Ganaoui, Buoyancy effects on upward and downward laminar mixed convection heat and mass transfer in a vertical channel, Int. J. Numer. Methods Heat Fluid Flow 17 (2007) 333–353.
[23] T. Fujii, Y. Kato, K. Mihara, Expressions of transport and thermodynamic properties of air, steam and water, Sei San Ka Gaku Ken Kyu Jo, Report No. 66, Kyu Shu University, Kyu Shu, Japan, 1977.
[24] D.R. Lide, H.V. Kehiaian, CRC Handbook of Thermophysical and Thermophysical Data, CRC Press, Boca Raton, FL, 2001.
[25] R.B. Bird, W.E. Stewart, E.N. Lightfoot, Transport Phenomena, Wiley, New York, 1960.